Journal of Statistical Physics, Vol. 64, Nos. 5/6, 1991

The Effect of a Coriolis Force on Taylor–Couette Flow

Richard J. Wiener,[1] Philip W. Hammer,[1] Charles E. Swanson,[1] David C. Samuels,[1] and Russell J. Donnelly[1]

Taylor–Couette flow subject to a Coriolis force is studied experimentally and numerically. In the experiment, the Couette apparatus is mounted on a turntable with the axis of the cylinders orthogonal to the rotation vector of the turntable. The Coriolis force stabilizes the fluid against the onset of Taylor vortices and alters the velocity fields, both above and below the transition from the initial flow. At small dimensionless turntable frequencies Ω, the transition yields time-independent Taylor vortices which are tilted with respect to the cylinder axis. At larger Ω there is a direct transition to turbulence. We determine the first-order correction to the classical Couette initial flow, to account for the effects of the Coriolis force, by expanding in powers of Ω. We present numerical results for the axial velocity (the only nonvanishing correction term to order Ω) in the infinite-cylinder approximation.

KEY WORDS: Taylor–Couette flow; Coriolis force; onset of instability; direct transition to turbulence; tilted Taylor vortex flow; Navier–Stokes equation in a rotating reference frame.

1. INTRODUCTION

Coriolis effects occur widely in nature, and often play a crucial role in the dynamics of fluid flows. For instance, the Coriolis force which arises from the earth's rotation profoundly impacts atmospheric flows,[1] and rotating convective systems display significant Coriolis effects.[2–7] One strategy to gain insight into the basic fluid dynamics resulting from this force is to investigate its effects on simple hydrodynamic systems with well-defined geometries and control parameters. In the current investigation we are

[1] Department of Physics, University of Oregon, Eugene, Oregon 97403.

822/64/5-6-2

exploring the effect of a Coriolis force on Taylor–Couette flow, which is the flow of fluid between concentric rotating cylinders.[8]

The Coriolis force is applied by mounting a Couette apparatus on a turntable with the axis of the cylinders orthogonal to the rotation vector of the turntable.[9] This orientation is chosen instead of aligning the axis of the cylinders parallel to the table rotation vector, since we believe that the latter arrangement simply adds the angular frequency of the turntable to the angular frequencies of the cylinders, which does not differ from ordinary Taylor–Couette flow. The centrifugal force does not affect the dynamics of the system, since it is balanced by an adverse pressure gradient.[1] We discuss this point in greater detail in Section 4.

One advantage of introducing a Coriolis force into a system, beyond gaining understanding into its effects, is the addition of a second control parameter. Additional parameters are intrinsically interesting in that they may influence the onset of instability and lead to new dynamical behavior such as the Küppers–Lortz instability[5] or pattern formation near a codimension-2 point (see, e.g., ref. 10). In our experiment the outer cylinder is held fixed. Thus there are two control parameters, the angular frequency of the inner cylinder and the angular frequency of the turntable. The former is scaled by the Reynolds number $Re = \omega R_1 d/\nu$, where ω is the angular frequency of the inner cylinder, $d = R_2 - R_1$ is the gap size, R_1 and R_2 are the inner and outer cylinder radii, and ν is the kinematic viscosity. Ω_D, the angular frequency of the turntable, is scaled by the dimensionless rotation rate, $\Omega = \Omega_D d^2/\nu$. Here Ω is the inverse of the Ekman number[1] and indicates the ratio of the Coriolis force to the viscous force.

In the geostrophic limit, where the inertial and viscous forces are small compared to the Coriolis force, the Taylor–Proudman theorem shows that the flow cannot change its velocity in the direction parallel to the rotation vector of the turntable.[1,2] But the onset of Taylor vortices requires such changes in velocity. This limiting case suggests that the Coriolis force should stabilize the fluid against the onset of Taylor vortices, in the sense that the fluid must be driven harder (i.e., the Reynolds number must be greater) for the transition to occur. The data confirm this qualitative behavior.[9]

In this paper we discuss qualitative and quantitative experimental results, with specific emphasis on the stability of the initial flow. We also discuss some of the changes the Coriolis force induces in the flow fields. In particular, the Coriolis force perturbs the Taylor vortices, and at high Ω there is a direct transition to turbulence from the initial flow.

Linear stability analysis is one method to calculate the stability of the initial flow.[2] However, the Coriolis force breaks the azimuthal symmetry of the classical Couette initial flow. The broken symmetry complicates the

stability analysis. We derive the first-order approximation to the equations for the initial flow and numerically solve these equations, as a first step toward a linear stability analysis.

2. EXPERIMENTAL SETUP

We use a Couette apparatus with an outer-cylinder radius R_2 equal to 2.54 cm. Most data points were collected with the radius ratio $\eta = R_1/R_2$ equal to 0.883. Some work was done with $\eta = 0.950$, in order to investigate radius ratio effects. The aspect ratio $\Gamma = L/d$, where L is the length of the annulus, is 70 for data taken with $\eta = 0.883$ and 167 for those taken with $\eta = 0.950$.

The working fluid is an aqueous glycerol solution, seeded with 2% Kalliroscope and 1% stabilizer, by volume. Different concentrations of glycerol and water were used to vary the kinematic viscosity over an order of magnitude, from approximately 0.011 to 0.11 Stokes. Details of the determination of ν and temperature control are included in ref. 9.

Kalliroscope is a nearly neutrally buoyant tracer, composed of platelets which align with the shear of the flow, and it is used for flow visualization. An infrared beam is fixed so that it reflects from the Kalliroscope at a point halfway between the ends of the cylinders. The intensity of the reflected beam forms the quantitative information for the experiment. A relatively high reflectance indicates that the platelets are aligned with a primarily azimuthal flow, i.e., the initial flow. A radial velocity component begins to grow at the transition to secondary flow, and some of the platelets intercept the beam edge on, resulting in a lowered reflectance.[9,11]

Reference 9 describes our experimental protocol and explains how the control parameters were varied to acquire data.

3. EXPERIMENTAL RESULTS

The Coriolis force stabilizes the fluid against the onset of secondary flow. We present some experimental results for the stability of the initial flow. We also show results for Coriolis effects on secondary flows.

3.1. Stability of the Initial Flow

Figure 1 shows relative reflectance data plotted as a function of Re for a constant value of the second control parameter, $\Omega = 1.5$, at $\eta = 0.883$. Each datum is a mean of reflectance measurements taken with both control parameters constant. The squares indicate data between which Re was

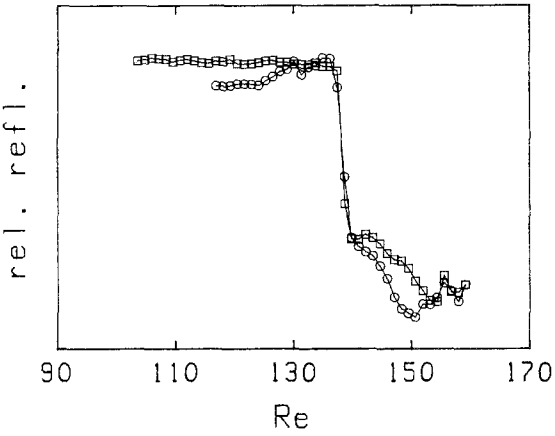

Fig. 1. Relative reflectance data as a function of Re with $\eta = 0.883$.

quasistatically increased; the circles indicate quasistatic decrease between points. (References 9, 11, and 12 discuss the criterion for "quasistatic.") The large change in reflectance corresponds to the transition from initial to secondary flow. We take the value of Re corresponding to a 10% drop in reflectance from its upper to its lower asymptotic value to be the critical Reynolds number for the onset of instability, Re_c. The determination of the asymptotic values of reflectance is somewhat uncertain, particularly at higher values of Ω. This uncertainty contributes to the error in Re_c. Figure 1 indicates that $Re_c \approx 138$ is greater for the nonzero value of Ω than $Re_{c0} = 121.9$, where Re_{c0} is the critical Reynolds number in the absence of a Coriolis force.

Figure 2 shows a plot of the stability curve constructed from a series of relative reflectance versus Reynolds number plots as in Fig. 1. The ordinate represents the fractional change in the critical Reynolds number $\Delta = (Re_c - Re_{c0})/Re_{c0}$. The quantity Δ is known to greater accuracy than absolute values of the various fluid parameters entering into the Reynolds number. $\Delta > 0$ indicates stabilization. Thus, Fig. 2 shows that the Coriolis force stabilizes the flow. Stabilization is quite pronounced even for small table rotation rates. For example, Re_c is twice Re_{c0} at $\Omega \approx 4.2$. These values correspond to a ratio of the control parameters $\Omega_D/\omega = 0.13$; and $\Omega_D/2\pi \approx 0.08$ Hz for a fluid with $\nu = 0.01$ Stokes.

The symmetry of the system suggests that Δ should depend on the magnitude of Ω only, and not its direction; i.e., the change in the critical Reynolds number should be the same if table rotation is clockwise or counterclockwise. We have confirmed this result experimentally. The symmetry also explains the initial qualitative dependence of Δ on Ω. The

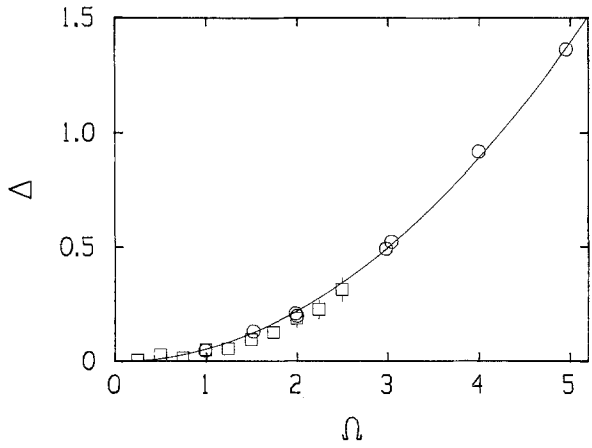

Fig. 2. Fractional change in the critical Reynolds number versus Ω for small Ω with $\eta = 0.883$, $\nu = 0.11$ S (squares), and $\nu = 0.011$ S (circles). The curve is a best fit of our data for $\Omega < 5$ to $\Delta = k\Omega^2$, $k = 0.0558 \pm 0.0005$.

curve in Fig. 2 is a best fit of our data to $\Delta = k\Omega^2$ at small values of Ω. This is consistent with a Taylor expansion of Re_c as a function of Ω, where the odd-order terms are zero due to symmetry. The quadratic dependence of Δ on Ω is analogous to the initial dependence of the fractional change in the critical Rayleigh number on Ω in rotating Rayleigh–Bénard convection,[2] which is also symmetric with respect to the direction of rotation.

At approximately $\Omega > 5$, Δ no longer scales as Ω^2. Instead, Δ increases monotonically, but less rapidly. In a previous paper, we concluded that Δ asymptotically scales as $Ta^{2/3}$, where $Ta = 4\Omega^2$ is the Taylor number.[9] This conclusion was based on data with Ta less than about 400 ($\Omega < 10$). We have subsequently taken data up to $\Omega \approx 22$ (Fig. 3). The $Ta^{2/3}$ ($\Omega^{4/3}$) scaling does not hold, and no simple power-law scaling is evident. At $\Omega \approx 22$, Re_c is close to seven times greater than Re_{c0}.

We found that the strength of stabilization depends on the radius ratio η. Stabilization is stronger for $\eta = 0.950$ than for $\eta = 0.883$. Our results at both radius ratios show that initially Δ is quadratic in Ω. Results of Ning *et al.*[13] at $\eta = 0.75$ also indicate initial quadratic stabilization, which is weaker than stabilization for our data at $\eta = 0.883$. This suggests that stability increases monotonically with η over the range of $\eta = 0.75$–0.95.

3.2. Direct Transition to Turbulence

The Coriolis force alters the velocity fields, both above and below the transition from initial flow. In this subsection we discuss experimental

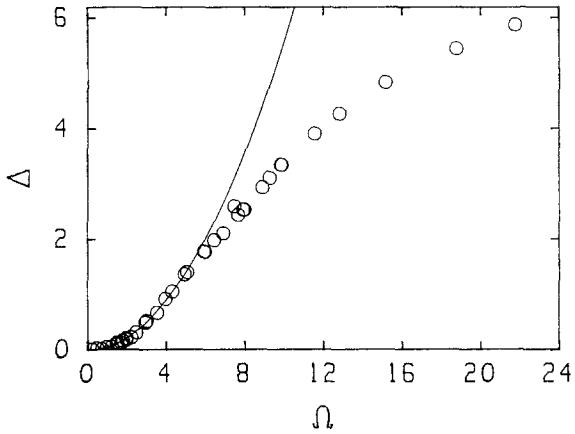

Fig. 3. Δ versus Ω with $\eta = 0.883$. The curve is the same fit as Fig. 2.

results concerned with the effect on secondary flows. In Section 4 we consider numerical results for the effect on the initial flow.

Above the transition, at small Ω, visual observation indicates that the Taylor vortices are tilted and the flow appears time-independent. We call this dynamical regime *tilted Taylor vortex flow*, TTVF, to distinguish it from ordinary Taylor vortex flow. Figure 4a is a plot of both the mean relative reflectance (as in Fig. 1) and the variance of the reflectance versus the Reynolds number, for $\Omega \approx 1$ ($Re_c \approx 129$). There is no significant change in the variance at the transition to TTVF from the time-independent initial flow, which we interpret as an indication that TTVF is time-independent. At $Re \approx 144$ the variance rises sharply, and coincides with our observation of the onset of time-dependent wavy vortex flow on the tilted vortices.

Reflectance data in Fig. 4b make the transition to secondary flow appear broader and less sharp than the transition in Fig. 4a. Visual observation indicates that the secondary flow is highly turbulent for $\Omega = 6.9$, the value for Fig. 4b. The Taylor vortices still exist, but they appear to be mixing chaotically. Much of the spatial periodicity characteristic of ordinary Taylor–Couette flow, even in the turbulent regime, is gone. The coincidence of the rise in variance with the drop in reflectance shows that there is a direct transition to time-dependent flow at the onset of secondary flow. In other words, a sufficiently strong Coriolis force eliminates the ordinary sequence of regimes leading to turbulence, including wavy vortex and modulated wavy vortex flow.

In Fig. 5 we plot Re_t/Re_c against Ω for data with $\eta = 0.883$, where Re_t is the critical Reynolds number for the onset to time-dependent flow. For all $\Omega \geqslant 5.3$, $Re_t/Re_c = 1$, indicating a direct transition to time dependence.

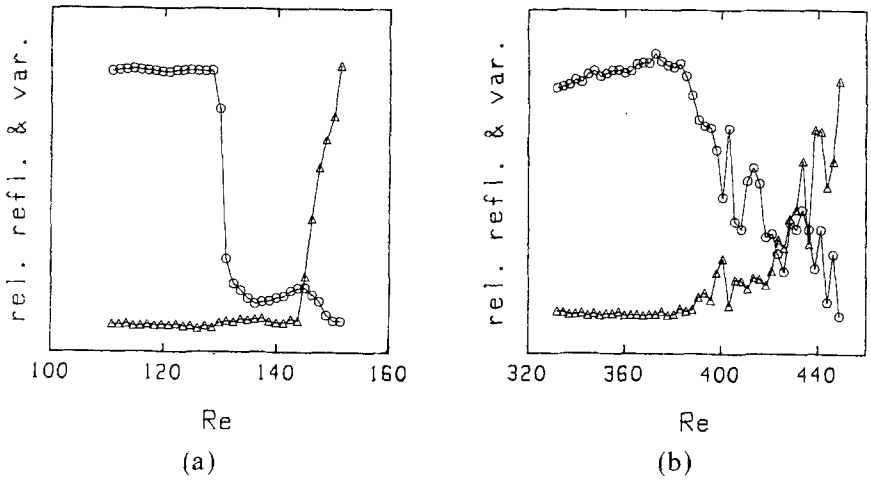

Fig. 4. (a) Relative reflectance (circles) and variance in the relative reflectance (triangles) plotted against Re for $\Omega = 1$ with $\eta = 0.883$; (b) the same for $\Omega = 6.9$. For clarity, only the points between which Re was quasistatically decreased are shown.

We have fit a line to the data where the ratio is greater than one in order to extrapolate this value of Ω. Interestingly, $\Omega \approx 5.3$ for the break from the region of quadratic scaling (Fig. 3).

4. NUMERICAL RESULTS FOR THE INITIAL FLOW

In this section we determine the first-order correction to Couette flow, which results from the Coriolis force, by expanding in powers of Ω to

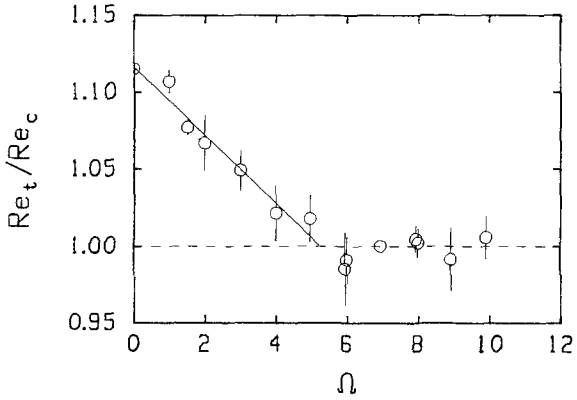

Fig. 5. Re_t/Re_c as a function of Ω, where Re_t is the critical Reynolds number for the onset of time dependence.

derive approximate equations for the initial flow. We present numerical results for the solution to these equations. We note that Brand[14] has independently carried out the derivation of the approximate equations.

Figure 6 is a defining diagram for a coordinate system when the Couette system is rotating about an axis orthogonal to the axis of the cylinders. The x axis is taken as the axis of rotation for the system, and the z axis as the axis of rotation for the inner cylinder. This choice of coordinates allows for the use of cylindrical coordinates to describe position and velocity in the annulus. The rotation vector of the system $\boldsymbol{\Omega}_D$ can be written in cylindrical coordinates as

$$\Omega_D \hat{x} = \Omega_D(\hat{r}\cos\phi - \hat{\phi}\sin\phi) \tag{1}$$

where $\hat{x}$, $\hat{r}$, and $\hat{\phi}$ are unit vectors in the x, radial, and azimuthal directions, respectively. If we adopt a rotating frame of reference in which the Couette system is stationary, the continuity and steady-state Navier–Stokes equations are

$$\nabla \cdot \mathbf{u} = 0 \tag{2}$$

$$\mathbf{u} \cdot \nabla \mathbf{u} = -\nabla P + \frac{1}{Re}(\nabla^2 \mathbf{u} - 2\boldsymbol{\Omega} \times \mathbf{u}) \tag{3}$$

Equations (2) and (3) are written in terms of dimensionless variables, where we assume a characteristic length scale $L = d$, the gap size, and

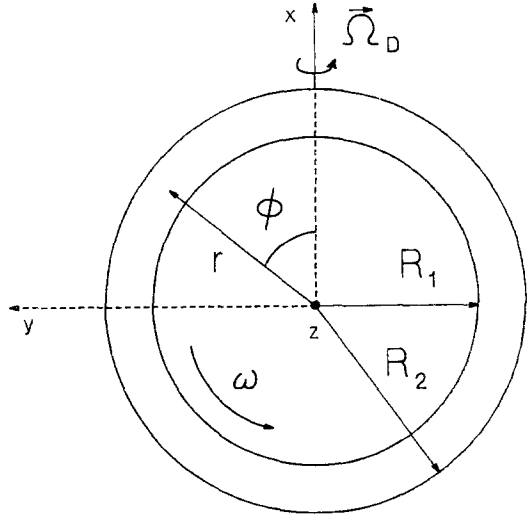

Fig. 6. Defining diagram for the coordinate system. The z axis is out of the paper.

velocity scale $U=\omega R_1$, the inner-cylinder velocity. $Re=\omega R_1 d/\nu$ is the Reynolds number and $\mathbf{\Omega}=\mathbf{\Omega}_D d^2/\nu$ is the dimensionless rotation vector of the rotating reference frame. P represents an effective dimensionless pressure that includes the centrifugal force, which is equal to a scalar potential. The procedure of subsuming the centrifugal force in P implies that this force plays no role in the dynamics of the system.[2] This is analogous to subtracting out the hydrostatic head due to gravity. The conditions for this procedure to be valid are that the pressure does not appear explicitly in the boundary conditions and the density of the fluid is constant.[1]

In the infinite-cylinder approximation, with the outer cylinder fixed, the boundary conditions for Eqs. (2) and (3) are

$$\begin{aligned} &\text{inner cylilnder:} \quad r=\eta/(1-\eta) \\ &u_r=0, \qquad u_\phi=1, \qquad u_z=0 \\ &\text{outer cylinder:} \quad r=1/(1-\eta) \\ &u_r=0, \qquad u_\phi=0, \qquad u_z=0 \end{aligned} \tag{4}$$

where $\eta=R_1/R_2$ is the radius ratio.

Couette flow, the classical initial flow in the absence of the Coriolis force, is azimuthal, with the velocity and pressure dependent only on radial position,

$$u_{z0}=u_{r0}=0 \tag{5}$$

$$u_{\phi 0}=Ar+B/r \tag{6}$$

$$\frac{dP_0}{dr}=\frac{u_{\phi 0}^2}{r} \tag{7}$$

where A and B are constants determined by the boundary conditions.[3]

We carry out the power expansion in terms of small Ω by assuming that the components of the velocity and the pressure for the initial flow are each corrected by a small term of order Ω,

[2] We have checked experimentally that the centrifugal force does not affect the dynamics of the flow, by measuring the angle of the tilt in TTVF for apparatus radially on center and one off center. We found that the angle does not depend on the radial position or orientation of the system. In addition, Ning *et al.*[13] found that the stability behavior does not change for radially centered and noncentered systems.

[3] In terms of dimensionless variables, where $u_{\phi 0}$ has been scaled by ωR_1, r has been scaled by $d=R_2-R_1$, and $\eta=R_1/R_2$, $A=-\eta/(1+\eta)$ and $B=\eta/[(1-\eta)(1-\eta^2)]$.

$$u_z = u_{z0} + \Omega u_{z1} = \Omega u_{z1} \tag{8}$$

$$u_r = u_{r0} + \Omega u_{r1} = \Omega u_{r1} \tag{9}$$

$$u_\phi = u_{\phi 0} + \Omega u_{\phi 1} \tag{10}$$

$$P = P_0 + \Omega P_1 \tag{11}$$

These equations are then substituted back into the continuity and Navier–Stokes equations, Eqs. (2) and (3). The infinite-cylinder approximation implies that all z dependence is negligible. Using Eqs. (1) and (8)–(10), we find that the cross product in the Navier–Stokes equation is

$$\begin{aligned} -2\boldsymbol{\Omega} \times \mathbf{u} = & -2\Omega(-\hat{r}\Omega u_{z1} \sin\phi - \hat{\phi}\Omega u_{z1} \cos\phi \\ & + \hat{z}\Omega u_{r1} \sin\phi + \hat{z}\Omega u_{\phi 1} \cos\phi \\ & + \hat{z} u_{\phi 0} \cos\phi) \end{aligned} \tag{12}$$

Only the last term on the right-hand side of Eq. (12) is first order in Ω. All other terms are second order. Thus, the first-order effect of the Coriolis force is given by the interaction of Ω and the azimuthal initial flow. The term which represents this interaction appears in the axial component of the Navier–Stokes equation. This suggests that the axial velocity is the only nonvanishing first-order correction term to the initial flow. Thus we make the following Ansatz, which is justified *a posteriori*,

$$u_{r1} = u_{\phi 1} = P_1 = 0 \tag{13}$$

After substituting Eqs. (8)–(11) into Eqs. (2) and (3) and neglecting terms of second order, the continuity equation and the radial and azimuthal components of the Navier–Stokes equation are satisfied by classical Couette flow, Eqs. (5)–(7), and Eq. (13). The only remaining component of the Navier–Stokes equation is

$$\frac{u_{\phi 0}}{r}\frac{\partial u_{z1}}{\partial \phi} = \frac{1}{Re}\left(\frac{\partial^2 u_{z1}}{\partial r^2} + \frac{1}{r}\frac{\partial u_{z1}}{\partial r} + \frac{1}{r^2}\frac{\partial^2 u_{z1}}{\partial \phi^2} - 2u_{\phi 0}\cos\phi\right) \tag{14}$$

Equation (14) can be satisfied by an axial velocity of the form

$$u_{z1} = f(r)\cos\phi + g(r)\sin\phi \tag{15}$$

where $f(r)$ and $g(r)$ are functions of r alone. The $\cos\phi$ dependence of the Coriolis force term in Eq. (14) requires that the higher harmonics of u_{z1} are not excited. Substituting Eq. (15) into Eq. (14) and equating the coefficients of $\cos\phi$ and $\sin\phi$, respectively, yields two second-order, coupled, linear,

inhomogeneous, ordinary differential equations. If we denote differentiation with respect to r by a prime symbol, then

$$f'' + \frac{f'}{r} - \frac{f}{r^2} - \frac{Re}{r} u_{\phi 0}\, g = 2u_{\phi 0} \tag{16}$$

$$g'' + \frac{g'}{t} - \frac{g}{r^2} + \frac{Re}{r} u_{\phi 0} f = 0 \tag{17}$$

where $u_{\phi 0}$ is the azimuthal (and only nonzero) component of the classical Couette initial flow. In order to satisfy the boundary conditions, Eq. (4), f and g must each go to zero at the inner and outer cylinders, which gives four boundary conditions for Eqs. (16) and (17). The solution to these equations gives the first-order correction to the initial flow, when substituted into Eq. (15) and multiplied by Ω.

We solve Eqs. (16) and (17) using a shooting method for boundary value problems, which involves iteration of a standard fourth-order Runge-Kutta integration until the boundary values agree to within an arbitrary tolerance, which we chose as 10^{-10}.[15],[4] The quantity u_{z1} can be expressed in a more physically meaningful form as

$$u_{z1} = a(r)\cos[\phi + \delta(r)] \tag{18}$$

where $a(r) = [f^2(r) + g^2(r)]^{1/2}$ is the amplitude and $\delta(r) = \tan^{-1}[g(r)/f(r)]$ is the phase of u_{z1}. In Fig. 7 we plot $a(r)$ and $\delta(r)/\pi$ as a function of the radial position in the annulus for $Re = 128$, which is very near the critical Reynolds number for the onset of Taylor vortices at $\Omega = 1$. The amplitude is relatively strong across the middle of the gap, and zero at the inner and outer cylinders as required by the boundary conditions. The maximum amplitude is offset toward the inner radius and is less than 10% of the value of the inner-cylinder velocity, ωR_1 (assuming $\Omega = 1$). This suggests that second-order velocities may be less than 1% of ωR_1 for these values of Re and Ω. The position of the maximum is not surprising, since the azimuthal velocity which interacts with the rotation of the system to produce a Coriolis force is greatest at the inner cylinder. The phase has a relatively flat profile, and the maximum phase (in this case almost $\pi/4$) has nearly the same radial position as the maximum amplitude.

Figure 8 is a plot of the maximum amplitude $a_{\max}$ against Re at a constant Ω. Figure 8 shows that $a_{\max}$, which is scaled by the inner cylinder

[4] The solutions were checked by numerically taking the derivatives of f and g point by point, and substituting the results back into the differential equations. Typically the second derivatives given by the equations agree with the numerical second derivatives within a few percent.

velocity, increases with decreasing Reynolds number. To recover the physical (i.e., dimensioned) maximum amplitude, one must multiply $a_{\max}$ by ωR_1, which vanishes as Re goes to zero. The data indicate that $a_{\max}$ increases less rapidly than $1/Re$ as Re decreases. Thus, the physical amplitude vanishes at $Re = 0$, as it must. The inverse relationship between

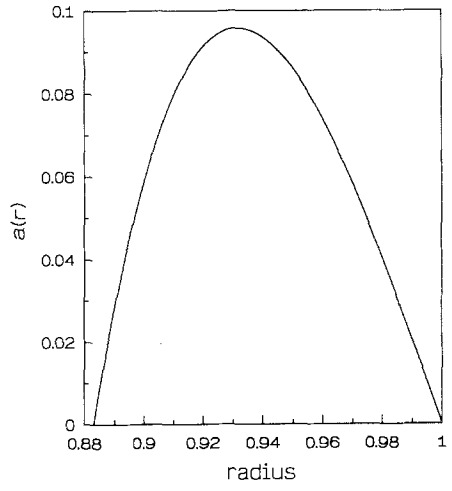

(a)

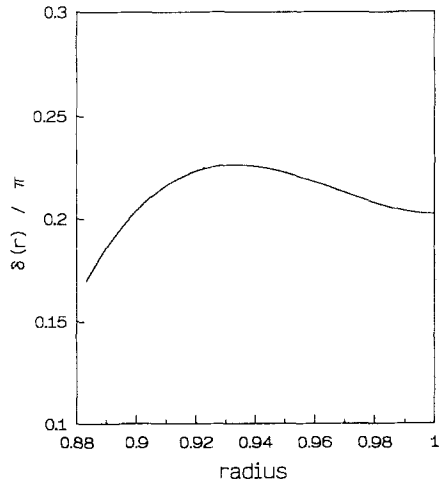

(b)

Fig. 7. (a) Plot of $a(r)$ versus the radius r; (b) $\delta(r)/\pi$ versus r. The inner- and outer-cylinder radii, $\eta(1-\eta) = 7.55$ and $1/(1-\eta) = 8.55$, are scaled to 0.883 and 1, respectively, and $a(r)$ is scaled by the inner-cylinder velocity, ωR_1.

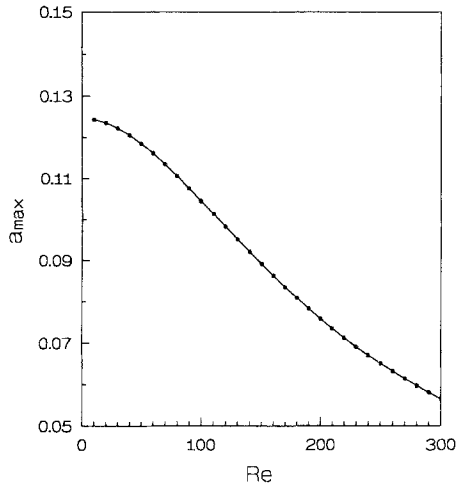

Fig. 8. The maximum amplitude a_{max} as a function of Re with constant $\Omega = 1$.

a_{max} and Re is very intriguing in light of the linear relationship between a_{max} and Ω. It shows that already in the initial flow, the two control parameters Re and Ω have competitive effects. This result is similar to competitive effects between the control parameters which we are observing in our ongoing investigation of secondary flow regimes.

5. CONCLUSION

Taylor–Couette flow subject to a Coriolis force is a novel variant of this fundamental system. The stability of the initial flow is markedly increased by the Coriolis force. At a high enough rotation rate Ω, the initial flow bifurcates directly to strong spatiotemporal turbulence. The transition to turbulence no longer involves singly- and doubly-periodic intermediate regimes as in ordinary Taylor–Couette flow.

Numerical results for an approximate solution to the initial flow offer clear, experimentally testable predictions. These results also constitute a first step toward a linear stability analysis of the initial flow.

ACKNOWLEDGMENTS

We wish to express our sincere thanks to Dr. Randall Tagg for stimulating discussions which led to the numerical results presented in this paper. We would also like to thank Profs. Helmut Brand, Guenter Ahlers,

and David Cannell and Li Ning for thoughtful exchanges on our investigation and their parallel work. This research is supported through NSF grant DMR-8815803.

REFERENCES

1. D. J. Tritton, *Physical Fluid Dynamics* (Clarendon Press, Oxford, 1988).
2. S. Chandrasekhar, *Hydrodynamic and Hydromagnetic Stability* (Clarendon Press, Oxford, 1961); *Proc. Am. Acad. Arts Sci.* **86**:323 (1957).
3. D. Fultz, Y. Nakagawa, and P. Frenzen, *Phys. Rev.* **94**:1471 (1954).
4. H. T. Rossby, *J. Fluid Mech.* **36**:309 (1969).
5. G. Küppers and D. Lortz, *J. Fluid Mech.* **35**:609 (1969).
6. R. M. Clever and F. H. Busse, *J. Fluid Mech.* **94**:609 (1979).
7. J. J. Niemela and R. J. Donnelly, *Phys. Rev. Lett.* **57**:2524 (1986).
8. R. C. Di Prima and H. L. Swinney, in *Hydrodynamic Instabilities and the Transition to Turbulence*, H. L. Swinney and J. P. Gollub, eds. (Springer-Verlag, Berlin, 1985).
9. R. J. Wienes, P. W. Hammer, C. E. Swanson, and R. J. Donnelly, *Phys. Rev. Lett.* **64**:1115 (1990).
10. Proceedings of the Conference on multiparameter Bifurcations, *Contemp. Math.* **56**:277 (1986).
11. T. J. Walsh, W. T. Wagner, and R. J. Donnelly, *Phys. Rev. Lett.* **58**:2543 (1987).
12. K. Park, G. L. Crawford, and R. J. Donnelly, *Phys. Rev. Lett.* **47**:1488 (1981).
13. L. Ning, G. Ahlers, and D. S. Cannell, *J. Stat. Phys.*, this issue.
14. H. Brand, private communication.
15. S. D. Conte and C. de Boor, *Elementary Numerical Analysis* (McGraw-Hill, New York, 1980).